THE JOURNAL OF PHYSICAL CHEMISTRY C

Article

pubs.acs.org/JPCC

Fluorescence Resonance Energy Transfer in Partially and Fully Labeled Pyrene Dendronized Porphyrins Studied with Model Free Analysis

Gerardo Zaragoza-Galán,[†] Michael Fowler,[‡] Regis Rein,[§,∥] Nathalie Solladié,*[,§,∥] Jean Duhamel,*[,‡] and Ernesto Rivera*[,⊥]

[†]Facultad de Ciencia Químicas, Universidad Autónoma de Chihuahua, Campus Universitario #2, Apartado Postal 669, Chihuahua 31125, Mexico

[‡]Institute for Polymer Research, Waterloo Institute for Nanotechnology, Department of Chemistry, University of Waterloo, Waterloo, Ontario N2L 3G1, Canada

[§]Laboratoire de Chimie de Coordination, CNRS, 205 route de Narbonne, BP 44099, F-31077 Toulouse Cedex 4, France

[∥]Université de Toulouse, UPS, INPT, F-31077 Toulouse Cedex 4, France

[⊥]Instituto de Investigaciones en Materiales, Universidad Nacional Autónoma de México, Ciudad Universitaria, Ciudad de México 04510 Distrito Federale, Mexico

Supporting Information

ABSTRACT: A series of dendronized porphyrins were synthesized and their photophysical properties were determined by UV−vis absorption, steady-state fluorescence, and time-resolved fluorescence. The constructs contained a porphyrin core connected to a first generation Fréchet-type dendron (Py_2G1) with or without a C_4-butanoate linker, and to a second generation dendron (Py_4G2) with a C_4-linker. Pyrene and porphyrin were selected as donor and acceptor, respectively, for fluorescence resonance energy transfer or FRET. FRET occurred efficiently within the dendronized porphyrins as determined from the extremely weak fluorescence of pyrene. The number of pyrene groups present in the constructs was varied from two to eight, but was found to have little effect on FRET as FRET took place efficiently from an excited pyrene to a ground-state porphyrin. The parameter that was found to affect FRET the most was the distance separating pyrene from porphyrin within a construct. This effect was probed successfully by fitting the pyrene and porphyrin fluorescence decays according to the model free analysis (MFA) which yielded the average rate constant $\langle k_{ET} \rangle$ for FRET. $\langle k_{ET} \rangle$ increased continuously with decreasing distance separating porphyrin and pyrene as determined by conducting molecular mechanics optimizations on the constructs. The $\langle k_{ET} \rangle$ values were used to determine the through-space distance d^{TS}_{Por-Py} separating porphyrin from pyrene. d^{TS}_{Por-Py} was found to scale as $(d^{EXT}_{Por-Py})^{0.5}$, where d^{EXT}_{Por-Py} represents the distance separating porphyrin and pyrene when the construct adopts its most extended conformation. This relationship suggests that FRET occurs intramolecularly inside the constructs between pyrene and porphyrin where both dyes are linked by a string of freely jointed Kuhn segments of length l_K = 9 Å.

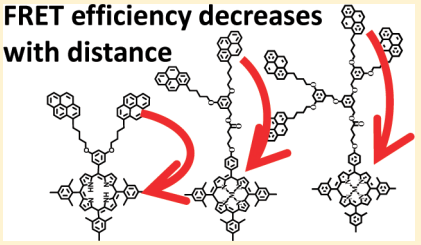

INTRODUCTION

The elucidation of the structure of the reaction center of purple bacteria has improved the comprehension of the photophysics in the early stages of photosynthesis.[1] With a deeper understanding of the light-harvesting and energy transfer processes that occur in natural chlorins, many chemists have been able to design more efficient materials for light energy conversion.[2−4] Special interest in porphyrins and multiporhyrinic systems has increased in past years because of their similarity to natural chlorins driving the very early stages of photosynthesis.[5,6] The ability of tuning the electronic properties of porphyrins by changing the meso positions or the coordination state of the macrocycle is a powerful tool to prepare new materials for specific applications.[5,6] Several functionalized porphyrins have been reported in the literature, and the chemistry of porphyrins is currently an active research area in both chemistry and materials science.[5−8] Photoactive molecules bearing pyrene moieties are of interest due to pyrene's peculiar photophysical properties[9,10] and its ability to π-stack with carbon nanotubes or graphene derivatives used in the construction of supramolecular nanohybrids.[11−15] The study of novel hybrids where pyrene-containing surfactants are used to stabilize an extended aromatic system such as carbon nanotubes or graphene could take advantage of recent advances in the development of kinetic models that describe the behavior of pyrene at the molecular level through fluorescence decay analysis. As presented in a number of recent reviews,[10,16,17] dynamic and structural information can now be obtained on

Received: February 10, 2014
Revised: March 17, 2014
Published: March 21, 2014

any type of pyrene labeled macromolecule by fitting the fluorescence decays of the pyrene monomer and excimer globally according to Birks' scheme,[18] the fluorescence blob model (FBM),[19] or model free analysis (MFA).[20] Whereas the application of Birks' scheme[18] and the FBM[19] is limited to the study of macromolecules that are labeled, respectively, by only two pyrenes at two specific positions or randomly with pyrene throughout the macromolecule, MFA is particularly interesting as it applies to any pyrene-labeled macromolecule regardless of the mode of pyrene labeling.[10,16,17]

Departing from its traditional use in the study of pyrene-labeled macromolecules,[10,16,17] MFA was recently applied to characterize the fluorescence resonance energy transfer (FRET) process between an excited pyrene located at the terminals of two Fréchet type pyrene-labeled dendrons of generation 1 (Py_2G1) and generation 2 (Py_4G2) and a ground-state porphyrin onto which the different dendrons had been covalently attached with a C_4-linker.[21] These constructs referred to as Por-C_4-Py_2G1 and Por-C_4-Py_4G2 were thoroughly characterized by steady-state and time-resolved fluorescence. The large Förster radius determined to be 5.2 nm for the pyrene−porphyrin donor−acceptor pair resulted from the substantial overlap between the fluorescence spectrum of the pyrene monomer and the absorption spectrum of porphyrin, the good fluorescence quantum yield of pyrene, and the large molar absorbance coefficient of porphyrin. The large Förster radius combined with the relatively small molecular dimension of these porphyrinic constructs consisting of a porphyrin at the core and a pyrene end-labeled dendron at the periphery ensured that efficient FRET took place between an excited pyrene monomer and a ground-state porphyrin yielding FRET efficiencies close to unity.

Interestingly, it was also found that the FRET process taking place within the porphyrinic constructs could not be characterized quantitatively through the analysis of the steady-state-fluorescence spectra acquired with the dendronized porphyrins. The minuscule fluorescence signal of minute traces of fluorescent impurities such as free pyrene-labeled dendrons competed with the equally minuscule fluorescence signal of the efficiently quenched pyrene donor thus distorting the fluorescence spectra. While steady-state fluorescence could not distinguish between the different forms of the chromophoric species present in solution, or more precisely whether pyrene was free in solution, attached to a free dendron, or attached to a free dendron itself being covalently connected to a porphyrin, time-resolved fluorescence could accurately assess the origin of each pyrene species by characterizing the individual temporal signature of each isolated chromophore. Taking advantage of the recent development of MFA, MFA was applied to describe quantitatively the complex FRET process taking place between an excited pyrene donor and a ground-state porphyrin acceptor located within the restricted macromolecular volume defined by these dendronized porphyrins. This study led to several important observations. First, in terms of time scale, global MFA of the fluorescence decays of the pyrene monomer and porphyrin demonstrated that FRET in the porphyrinic constructs occurred on so rapid a time scale that hardly any excimer could be generated between an excited and a ground-state pyrene monomer. Second, there was excellent agreement between the contributions to the fluorescence decays from the two chromophores pyrene and porphyrin constituting the dendronized porphyrins retrieved from MFA of the decays and the known chemical composition of the constructs. Finally, despite the large number of chromophore species located within the small macromolecular volume defined by the constructs, the energy appeared to be effectively localized on the individual chromophores with no indication of intramolecular ground-state complexation taking place between porphyrin and pyrene or between two pyrene monomers.

From a spectroscopic point of view, these earlier results confirmed that pyrene and porphyrin constitute an excellent donor−acceptor pair for FRET. From a material point of view, these experiments made clear that photon collection could be dramatically enhanced by increasing the number of donors present in the porphyrinic construct through the use of pyrene end-labeled dendrons, as many others have found before for different light-harvesting systems.[2−4] The combination of these two insights led to the conclusions that, first, the porphyrin−pyrene donor−acceptor pair could become a powerful feature to incorporate in the design of novel materials for light energy conversion and, second, attachment of increasing numbers of pyrene-labeled dendrons at the four meso positions of a porphyrin core would generate constructs that would maximize the absorption of the donor and the transfer of its excess energy to the porphyrin core. To this end, the four constructs Por-$(Py_2G1)_1$, Por-$(Py_2G1)_2$, Por-$(Py_2G1)_3$, and Por-$(Py_2G1)_4$ were prepared. The Py_2G1 dendron was preferred to Py_4G2 in order to reduce steric crowding during the synthesis of these four porphyrinic constructs. The C_4-linker used in the Por-C_4-Py_2G1 and Por-C_4-Py_4G2 constructs was removed for the Por-$(Py_2G1)_x$ ($x = 1 - 4$) series to shorten the donor−acceptor distance and maximize FRET. This paper describes the synthesis and characterization of the photophysical properties of the four porphyrinic constructs prepared with the Py_2G1 dendron and without the C_4-linker when the porphyrin is free or metalated with Zn. These results were compared to those obtained with Por-C_4-Py_2G1 and Por-C_4-Py_4G2 without or with Zn. This study provides a quantitative characterization of the complex photophysical behavior of these constructs and characterized quantitatively the effects that the number of pyrene donor groups and the pyrene−porphyrin distance have on the FRET process taking place intramolecularly within the macromolecular volume of these dendronized porphyrins.

EXPERIMENTAL SECTION

Distilled in glass tetrahydrofuran (THF, Caledon) was used in all fluorescence experiments. All the reagents involved in the synthesis were purchased from Aldrich and used as received. Solvents used in the reactions were purified by simple distillation. Py_2G1OH (**1**) was synthesized according to a previously reported procedure.[21] Fourier transform infrared (FTIR) spectra of the intermediates, dendrons, and pyrene−porphyrin dendritic systems were carried out on a Spectrum 100 (Perkin-Elmer) spectrometer in the solid state. ^1H and ^{13}C NMR spectra of these compounds were recorded in $CDCl_3$ at room temperature on a Bruker Avance 400 MHz spectrometer, operating at 400 and 100 MHz for ^1H and ^{13}C, respectively. Matrix-assisted laser desorption ionization time-of-flight (MALDI-TOF) measurements were conducted with a Bruker-MICROFLEX spectrometer.

Synthesis of Py_2G1CHO (3,5-Bis(4-pyren-1-yl-butoxy)-benzaldehyde) (2). To a solution of Py_2G1OH (**1**) (501 mg, 767 μmol) in 30 mL of THF, MnO_2 (806 mg, 9.3 mmol, 12 equiv) was added. The reaction mixture was stirred at room temperature under argon atmosphere for 16 h. After this time,

dx.doi.org/10.1021/jp501445n | J. Phys. Chem. C 2014, 118, 8280−8294

the solution was filtered over a celita plug and the solvent was evaporated under reduced pressure. The crude product was recrystallized from CH_2Cl_2:hexanes (1:1) and dried under vacuum. The pure compound was obtained as a white solid (Py_2G1CHO (**2**)) (429 mg, 659 μmol). Yield: 86%. ^{1}H NMR ($CDCl_3$, 400 MHz): δ (ppm) = 9.83 (Hα', s, 1H), 8.28−7.84 (HArPy, m, 18H), 6.93 (Ho, d, J = 2.25 Hz, 2H), 6.63 (Hp, t, J = 2.23 Hz, 1H), 3.97 (Hα, t, J = 7.57 Hz, 4H), 2.09−1.88 (Hβ and Hγ, m, 9H).

Synthesis of 2,2′-Mesityldipyrromethane (4). A mixture of pyrrole (47.7 g, 711 mmol, 40 equiv), mesitylaldehyde (2.6 g, 18 mmol), and $BF_3{\cdot}OEt_2$ (0.7 mL, 784 mg, 5,5 mmol, 0.3 equiv) was stirred at room temperature under argon atmosphere for 2 h. After this time, the solution was evaporated under vacuum at room temperature. The obtained dark-green oil was dissolved in a small amount of dichloromethane, washed with NaOH (0.1 M), and then washed with distilled water. The organic phase was evaporated under reduced pressure. The crude product was recrystallized from CH_2Cl_2:EtOH (9:1) and dried under vacuum. The desired product (DPM (**4**); 1.73 g, 6.5 mmol) was obtained as a pink solid with 37% yield. ^{1}H NMR ($CDCl_3$, 400 MHz): δ (ppm) = 7.94 (Hε, s, 2H), 6.87 (Hm, s, 2H), 6.67 (Hδ, s, 2H), 6.19 (Hγ, dd, 2H), 6.01 (Hβ, s, 2H), 5.93 (Hα, s, 1H), 2.29 (HA, s, 3H), 2.07 (HB, s, 6H).

Synthesis of Por-(Py_2G1)$_4$ (3a). G1CHO (512 mg, 787 μmol, 4 equiv) and pyrrole (53 mg, 787 μmol, 4 equiv) were dissolved in 72 mL of $CHCl_3$ previously dried over molecular sieves. A 32 μL volume of $BF_3{\cdot}OEt_2$ (36 mg, $C = 3.3 \times 10^{-3}$ M) was added and the mixture was stirred at room temperature under argon atmosphere for 1 h. Then, p-chloranil (145 mg, 0.6 mmol, 3 equiv) was added and the mixture was heated to reflux with stirring for 1.5 h. After this time, the mixture was cooled to room temperature, a few drops of NEt_3 were added to neutralize the acid, and the mixture was concentrated under vacuum. The crude product was purified by flash column chromatography on silica gel, using hexanes and then hexanes:dichloromethane (30:70) as eluent. The pure product (Por-(Py_2G1)$_4$ (**3a**)) was obtained as a purple solid (173 mg, 62 μmol). Yield: 32%. mp = >350 °C. ^{1}H NMR ($CDCl_3$, 400 MHz): δ (ppm) = 8.99 (Hα1, s, 8H), 8.14−7.70 (HAr-pyrene, m, 72H), 7.41 (Ho, s, 8H), 6.88 (Hp, s, 4H), 4.03 (Hα, m, 16H), 3.26 (Hδ, m, 16H), 1.91 (Hβ and Hγ, m, 32H), −2.51(Hβ1, s, 2H) . MS Calcd for $C_{204}H_{158}N_4O_8$ [M]+ m/z = 2792.21. Found MALDI-TOF MS: [M]+ m/z = 2792.36.

Synthesis of Por-(Py_2G1)$_2$ (5a). To a solution of Py_2G1CHO (**2**) (199 mg, 306 μmol, 2 equiv) in 30 mL of dried $CHCl_3$ containing 0.75% EtOH, dipyrromethane (**4**) (81 mg, 306 μmol, 2 equiv) and 13 μL of $BF_3{\cdot}OEt_2$ (14 mg, C = 3.3 0.10^{-3} M) were added. The reaction mixture was stirred at room temperature under inert atmosphere for 1 h. After addition of p-chloranil (226 mg, 920 μmol, 3 equiv), the refluxing mixture was stirred vigorously for 1.5 h. After completion of the reaction, the mixture was cooled to room temperature, a few drops of NEt_3 were added to neutralize the acid, and the resulting mixture was concentrated under reduced pressure. The crude product was purified by column chromatography on silica gel. The three products Por-(Py_2G1)$_3$ (**7**), Por-(Py_2G1)$_2$ (**5a**), and Por-(Py_2G1)$_1$ (**6**) were separated (hexane/CH_2Cl_2: from 50/50 to 0/100) from the reaction mixture.

Por-(Py_2G1)$_3$ (**7**) was purified using hexanes:dichloromethane (50:50) as eluent. Yield: 4%. ^{1}H NMR ($CDCl_3$, 400 MHz): δ (ppm) = 8.93 (Hα3 and Hα2, m, 6H), 8.67 (Hα1, d, J = 4.79 Hz, 2H), 8.23−7.75 (HArPy, m, 54H), 7.39 (Ho′, m, 6H), 7.27 (Hm, s, 2H), 6.87 (Hp′, t, J = 1.95 Hz, 3H), 4.12 (Hα, m, 12H), 3.36 (Hδ, m, 12H), 2.67 (HA, s, 3H), 2.67 (HA, s, 3H), 1.99 (Hβ and Hγ, m, 24H), −2.64 (Hβ1, s, 2H). MS Calcd for $C_{167}H_{132}N_4O_6$ [M]+ m/z = 2290.09. Found MALDI-TOF MS: [M]+ m/z = 2290.429.

Por-(Py_2G1)$_2$ (**5a**) was purified using hexanes:dichloromethane (30:70) as eluent, and 105 mg (153 mmol) of the purple solid was isolated with 38% yield. ^{1}H NMR ($CDCl_3$, 400 MHz): 8.95 (Hα1, d, J = 4.75 Hz, 4H), 8.71 (Hα2, d, J = 4.74 Hz, 4H), 8.29−7.84 (HArPy, m, 36H), 7.45 (Ho′, m, 4H), 7.30 (Hm, s, 4H), 6.91 (Hp′, m, 2H), 4.18 (Hα, t, J = 5.25 Hz, 8H), 3.40 (Hδ, t, J = 6.97 Hz, 8H), 2.66 (HA, s, 6H), 2.05 (Hβ and Hγ, m, 16H), 1.87 (HB, s, 12H), −2.54 (Hβ1, s, 2H). MS Calcd for $C_{130}H_{106}N_4O_4$ [M]+ m/z = 1787.82. Found MALDI-TOF MS: [M]+ m/z = 1787.767.

Por-(Py_2G1)$_1$ (**6**) was purified using hexanes:dichloromethane (20:80) as eluent. Yield: 2%. ^{1}H NMR ($CDCl_3$, 400 MHz): 8.87 (Hα2, d, J = 4.75 Hz, 2H), 8.64 (Hα3, d, J = 4.87 Hz, 2H), 8.62 (Hα1, d, J = 4.87 Hz, 4H), 8.29−7.85 (HArPy, m, 18H), 7.37 (Ho′, d,J = 2.16 Hz, 2H), 7.26 (Hm, s, 6H), 8.87 (Hp′, t, J = 2.09 Hz, 1H), 4.18 (Hα, t, J = 5.84 Hz, 4H), 3.42 (Hδ, t, J = 7.08 Hz, 4H), 2.62 (HA, s, 9H), 2.05 (Hβ and Hγ, m, 8H), 1.88 (HB, s, 18H), −2.55 (Hβ1, s, 2H). MS Calcd for $C_{93}H_{80}N_4O_2$ [M]+ m/z = 1285.63. Found MALDI-TOF MS: [M]+ m/z = 1285.585.

Absorption and Fluorescence Measurements. A Varian Cary 1 Bio UV/vis spectrophotometer was used to acquire the absorption spectra of the different compounds. Solutions of the porphyrin samples were prepared with concentrations of 3×10^{-6} and 8×10^{-5} M, and their absorption spectra were acquired with a 1 cm path length quartz cell to determine the molar absorbance coefficient of the constructs at the Soret band and at 344 nm, respectively. As reported in our earlier publication,[21] the fluorescence emitted by the dendronized porphyrins is extremely weak due to the efficient quenching of the excited pyrene by the porphyrin and the weak porphyrin fluorescence quantum yield. Consequently, special care was taken in the preparation of the solutions to ensure that the fluorescence signal emitted by the solutions was not corrupted by unwanted fluorescent impurities. A detailed description of the precautions adopted for sample preparation has already been published.[21] A Photon Technology International LS-100 steady-state fluorometer equipped with a continuous Ushio UXL-75Xe xenon arc lamp and a PTI 814 photomultiplier detection system was employed to acquire the steady-state-fluorescence spectra. The excitation wavelength was set at 344 nm, and the solutions were placed in a 1 × 1 cm^2 quartz cell. For the fluorescence measurements, the solutions were diluted until the absorbance at 344 nm was smaller than 0.05 in order to avoid the inner filter effect. An IBH Ltd. time-resolved fluorometer equipped with an IBH 340 nm NanoLED was used to acquire the fluorescence decays. As for the fluorescence spectra, the samples were excited at 344 nm and the monomer, excimer, and porphyrin fluorescence decays were acquired at 375, 510, and 650 nm, respectively. Cutoff filters at 370, 480, and 550 nm were used to block residual light scattering from reaching the detector during the acquisition of the fluorescence decays of the pyrene monomer, pyrene excimer, and porphyrin, respectively. A Ludox solution was used to determine the instrument response function. The model free analysis (MFA) was applied to fit the fluorescence decays. MFA has been described in a number of reviews.[10,16,17] Optimization of the

parameters retrieved through the MFA of the decays was accomplished with the Marquardt−Levenberg algorithm[22] according to eqs S1 and S2 given in the Supporting Information. The quality of the fits was determined from the χ^2 parameter ($\chi^2 < 1.30$) and the random distribution of the residuals and the autocorrelation of the residuals.

Determination of the Förster Radius. The Förster radius of the pyrene−porphyrin donor−acceptor pair was calculated for all constructs using eq 1.

$$R_o = 9790(\kappa^2 n^{-4} \phi_d J)^{1/6} \quad (1)$$

In eq 1, R_o is the Förster radius in angstroms, κ^2 is the orientation factor set to equal 2/3 assuming a random orientation of the emission and absorption dipole moments of the donor and acceptor, respectively, n is the refractive index of the solvent (1.4050 for THF), ϕ_d is the fluorescence quantum yield of the 1-pyrenebutoxy donor found to equal 0.524 in Table 1, and J is the overlap integral of the pyrene−porphyrin pair.[23] The normalized fluorescence spectrum of the donor was taken as that of 1-pyrenebutanol since the porphyrinic constructs generated very little excimer. Since only the porphyrin moiety absorbs significantly where pyrene emits, J was obtained by integrating the product of the normalized fluorescence spectrum of 1-pyrenebutanol with the spectrum of the molar absorbance coefficient of the constructs shown in Figure 4. The R_o values and fluorescence quantum yields of the pyrene monomer and porphyrin obtained for the dendronized porphyrins without or with Zn have been listed in Table 1.

Table 1. Förster Radii (R_o), Pyrene Monomer Quantum Yield (ϕ_{Py}), and Porphyrin Quantum Yield (ϕ_{Por}) Obtained by Exciting the Solutions at 344 nm

	without Zn			with Zn		
sample	R_o (Å)	ϕ_{Py} (×10⁴)	ϕ_{Por} (×10⁴)	R_o (Å)	ϕ_{Py} (×10⁴)	ϕ_{Por} (×10⁴)
Por-$(Py_2G1)_4$	51.4	6	15	48.3	1	27
Por-$(Py_2G1)_3$	51.8	16	15			
Por-$(Py_2G1)_2$	51.5	12	15	48.5	2	34
Por-$(Py_2G1)_1$	51.8	25	15			
Por-C_4-(Py_2G1)	52.0	13	14	48.9	12	39
Por-C_4-(Py_4G2)	52.0	18	14	49.0	23	38

RESULTS AND DISCUSSION

Synthesis of the Porphyrinic Constructs. The synthesis of the Por-C_4-Py_2G1 and Por-C_4-Py_4G2 constructs has been described earlier.[21] The covalent attachment of the Py_2G1 dendrons at the meso positions of the porphyrin macrocycle to yield Por-$(Py_2G1)_x$, where x = 1−4, is presented hereafter. Compounds Por-$(Py_2G1)_2$, Por-$(Py_2G1)_4$, Por-C_4-Py_2G1, and Por-C_4-Py_4G2 were further Zn-metalated to study the effect of coordination over the energy transfer properties. The structures of all porphyrins investigated in this study are illustrated in Figure 1, and the syntheses of the four new porphyrins without C_4-linker are shown in Figure 2.

The partially and fully labeled pyrene dendronized porphyrins were synthesized using the Lindsey protocol.[24] This methodology was chosen due to its ability to yield symmetric and asymmetric porphyrins from sensitive aldehydes, which are not affordable by employing other synthetic methods such as that of Rothemund and Alder−Longo.[25,26] Fully substituted porphyrin Por-$(Py_2G1)_4$ (**3a**) was obtained from direct condensation of Py_2G1CHO (**2**) and pyrrole under Lindsey's conditions in 32% yield. Commonly, the Lindsey reaction leads to the formation of all probable substituted porphyrins: Por-$(Py_2G1)_4$, Por-$(Py_2G1)_3$, *cis*-Por-$(Py_2G1)_2$, *trans*-Por-$(Py_2G1)_2$, Por-$(Py_2G1)_1$, and tetramesitylporphyrin (TME). However, it is possible to obtain a main product in good yield by employing the appropriate stoichiometry of the starting materials.[24,27] Since the isolation of the *cis*- and *trans*-Por-$(Py_2G1)_2$ isomers from the reaction mixture by standard chromatographic methods is complicated, an alternative selective methodology was employed to obtain the *trans*-Por-$(Py_2G1)_2$ (**5a**) compound by condensation of mesityldipyrromethane (**4**) and Py_2-G1CHO (**2**) using $BF_3{\cdot}OEt_2$ as acid catalyst. Por-$(Py_2G1)_2$ (**5a**) was obtained as a main product with 38% yield. It was also possible to isolate other partially substituted porphyrins from the reaction mixture, namely Por-$(Py_2G1)_1$ (**6**) and Por-$(Py_2G1)_3$ (**7**) with 2 and 4% yield, respectively, resulting from the partial acidolysis of mesityldipyrromethane (**4**). Structural characterization of the different porphyrins was conducted by simple inspection of the ^{1}H NMR spectra, since symmetry of the pyrrolic macrocycle is clearly distinguishable in the aromatic region. MALDI-TOF analysis confirmed that the desired products were obtained. Por-$(Py_2G1)_4$ (**3a**) and Por-$(Py_2G1)_2$ (**5a**) were zinc-metalated according to a method previously reported in the literature.[21]

Analysis of the Absorption Spectra. The absorption spectra of the porphyrinic constructs shown in Figure 1 were acquired in THF. They are shown in Figure 3. The absorbance spectra show the typical bands of the $S_0 \rightarrow S_2$ absorption of 1-pyrenebutanol centered at 313, 327, and 344 nm. The Soret bands of the free porphyrin and metalated porphyrin were found at ∼420 and ∼426 nm, respectively. Finally, all compounds exhibited four Q bands situated in the region between 513 and 647 nm. Replacing a pyrene-labeled dendron by a mesityl group induced a 1 nm blue shift of the position of the Soret band as shown in the insets of Figure 3A,B. For the free porphyrins, the Soret band shifted from 421 to 420, 419, and 418 nm when going from Por-$(Py_2G1)_4$ to Por-$(Py_2G1)_3$, Por-$(Py_2G1)_2$, and Por-$(Py_2G1)_1$. Similarly, the position of the Soret band was displaced from 427 to 425 nm for the metalated porphyrins when going from Zn-Por-$(Py_2G1)_4$ to Zn-Por-$(Py_2G1)_2$. The monosubstituted porphyrins Por-C_4-(Py_2G1) and Por-C_4-(Py_4G2) bearing a single Py_2G1 or Py_4G2 dendron separated from the porphyrin with a butanoate C_4-spacer showed the same absorption maximum located at 421 nm for the free porphyrins and 425 nm for the metalated porphyrins as presented in the insets of Figure 3C,D. The Soret band was broader for the free porphyrins yielding a full width at half-maximum (fwhm) of 13 nm versus 10 nm for the metalated porphyrins.

Since the absorption spectra of the free-base dendronized porphyrins were practically a sum of the absorption spectra of 1-pyrenebutanol and porphyrin, little to no electronic interactions were expected to take place between both photoactive chromophores. This was further confirmed by ^{1}H NMR spectra (Figures S1−S4 in the Supporting Information), which did not show any anisotropic shift resulting from interactions between the pyrene and porphyrin units. This conclusion could be employed to further confirm the chemical composition of the porphyrinic constructs already established by ^{1}H NMR and MALDI-TOF measurements in terms of the different chromophore species constituting these constructs.

dx.doi.org/10.1021/jp501445n | J. Phys. Chem. C 2014, 118, 8280−8294

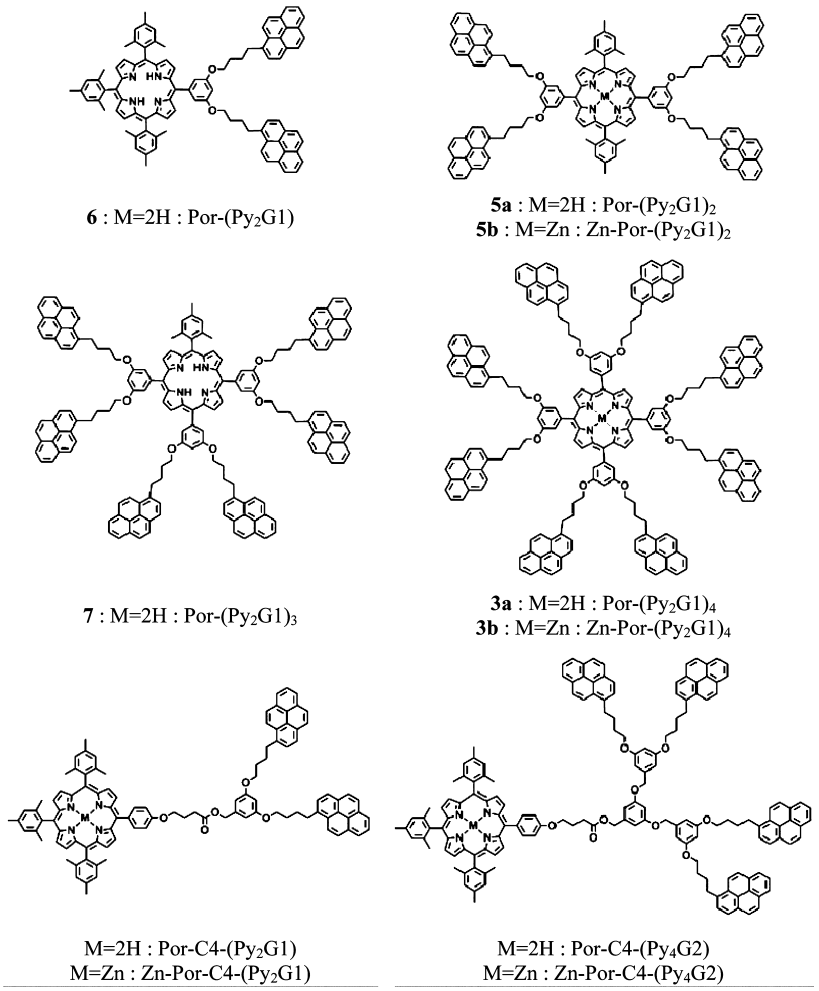

Figure 1. Pyrene dendronized porphyrins studied in this work.

This was achieved by plotting the ratios Abs(344 nm)/Abs(Soret) as a function of the number of pyrenyl units per porphyrinic construct as shown in Figure 3E,F for the free and metalated porphyrinic constructs, respectively. Since each porphyrinic construct possesses a single porphyrin unit, the Abs(344 nm)/Abs(Soret) ratio should be well represented by eq 2, which uses the molar absorbance coefficient of the 1-pyrenebutoxy derivative at 344 nm, ε_{Py}(344 nm), and those of the porphyrin unit at 344 nm and at the Soret band referred to as ε_{Por}(344 nm) and ε_{Por}(Soret), respectively.

$$\frac{\text{Abs}(344\text{ nm})}{\text{Abs}(\text{Soret})} = \frac{\varepsilon_{Por}(344\text{ nm})}{\varepsilon_{Por}(\text{Soret})} + n\frac{\varepsilon_{Py}(344\text{ nm})}{\varepsilon_{Por}(\text{Soret})} \quad (2)$$

As expected from eq 2, the Abs(344 nm)/Abs(Soret) ratio was found to increase linearly with increasing number of pyrenyl units. The excellent linear relationships shown in Figure 3E,F also supported the claim that porphyrin and pyrene do not form ground-state complexes intramolecularly as ground-state complexes would affect the absorbance of the pyrene and porphyrin chromophores which would result in a nonlinear response of the Abs(344 nm)/Abs(Soret) ratio with the number of pyrene labels. Knowing that the molar absorbance coefficient of 1-pyrenebutanol in THF equals 42 250 $M^{-1}\cdot cm^{-1}$,[21] the slopes and intercepts found in Figure 3E,F could be used to determine ε_{Por}(344 nm) and ε_{Por}(Soret) from the expression given in eq 2. For the free porphyrins, ε_{Por}(344 nm) and ε_{Por}(Soret) were found to equal 25 000 ± 5000 and 490 000 ± 13 000 $M^{-1}\cdot cm^{-1}$, whereas for the metalated porphyrins ε_{Por}(344 nm) and ε_{Por}(Soret) took values of 10 000 ± 8000 and 681 000 ± 25 000 $M^{-1}\cdot cm^{-1}$, respectively. ε_{Por}(Soret) values of 490 000 and 681 000 $M^{-1}\cdot cm^{-1}$ for free and metalated porphyrins are reasonable as confirmed by earlier reports.[28] Together, the successful analysis of the absorption spectra shown in Figure 3A−D based on eq 2 further confirmed the chemical composition of these constructs obtained by ^{1}H NMR and mass spectrometry.

Analysis of Fluorescence Spectra. After the stringent sample preparation reported in an earlier publication was followed,[21] the fluorescence spectra of the porphyrinic constructs were acquired and they are shown in Figure 4. The spectra were normalized so that their integral over the entire wavelength range reported in Figure 4 would yield their quantum yield. Direct comparison of the *Y*-axes on the left for the porphyrinic constructs and on the right for 1-pyrenebutanol in tetrahydrofuran with a fluorescence quantum yield of 0.52 illustrates how efficient FRET is between an excited 1-pyrenebutoxy and a ground-state porphyrinic moiety as the fluorescence intensity is decreased by more than 2 orders of magnitude.

The efficient FRET observed between the excited peripheral pyrene and the ground-state porphyrin core of these constructs is expected based on the fully extended center-to-center distance between a porphyrin and pyrenyl moiety (d^{EXT}_{Por-Py})

dx.doi.org/10.1021/jp501445n | J. Phys. Chem. C 2014, 118, 8280−8294

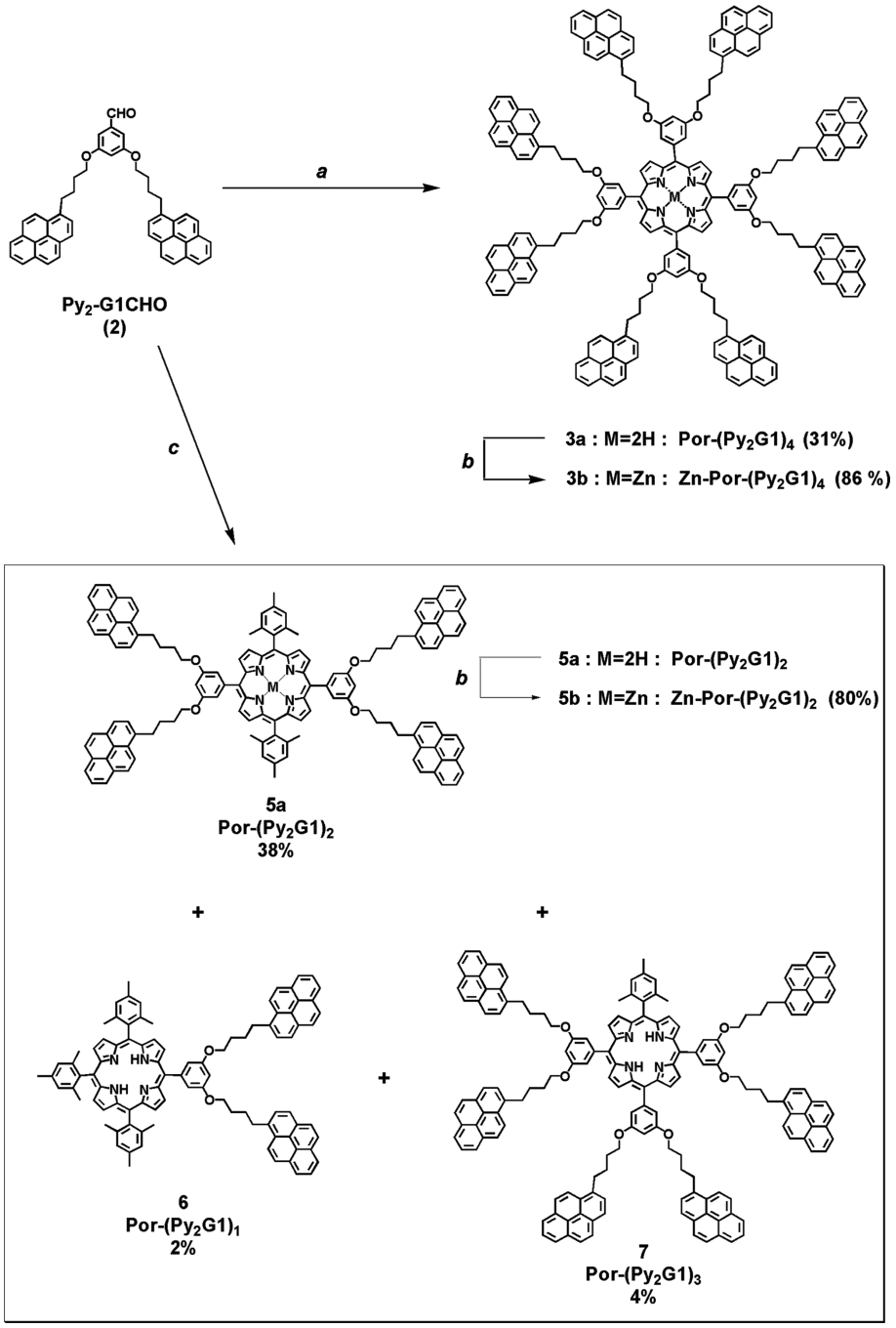

Figure 2. (a) Pyrrole, $BF_3{\cdot}OEt_2$, $CHCl_3$, room temperature, 1 h, then *p*-chloranil, reflux, 1.5 h, 32%. (b) $Zn(OAc)_2{\cdot}2H_2O$, $CHCl_3$, reflux, 1.5 h. (c) Dipyrromethane (**4**) 2 equiv, $BF_3{\cdot}OEt_2$, $CHCl_3$, room temperature, then *p*-chloranil, reflux, 1.5 h.

listed in Table 2 that ranges between 18 and 35 Å depending on the construct and the Förster radius (R_o) found to equal 51.8 ± 0.2 and 48.7 ± 0.3 Å in Table 1 depending on whether the porphyrin is free or metalated, respectively. The distance d^{EXT}_{Por-Py} was determined by conducting molecular mechanics optimizations with the program Hyperchem. Since d^{EXT}_{Por-Py} is much smaller than R_o for all porphyrin constructs, FRET is expected to occur on a time scale that is much faster than excimer formation within a Py_2G1 or Py_4G2 dendron.

This conclusion was confirmed experimentally in an earlier study using time-resolved fluorescence by applying model free analysis (MFA) to the fluorescence decays of the pyrene monomer and porphyrin of the Por-C_4-(Py_2G1) and Por-C_4-(Py_4G2) constructs.[21] Since an excited pyrenyl moiety transfers its excess energy so effectively to the porphyrin core that the excited pyrene monomer is deactivated before having had a chance to encounter a ground-state pyrene to form an excimer, the strong excimer signal centered at 480 nm observed in all fluorescence spectra shown in Figure 4 is unexpected. In fact, the existence of the excimer is a mere artifact resulting from the presence of small amounts of fluorescent impurities whose emission can only be observed thanks to the efficient quenching of pyrene by porphyrin in the porphyrinic constructs. These fluorescent impurities result from the presence in the solution of residual amounts of the building blocks that the constructs are constituted of, namely 1-pyrenebutanol, porphyrin, and the

dx.doi.org/10.1021/jp501445n | J. Phys. Chem. C 2014, 118, 8280−8294

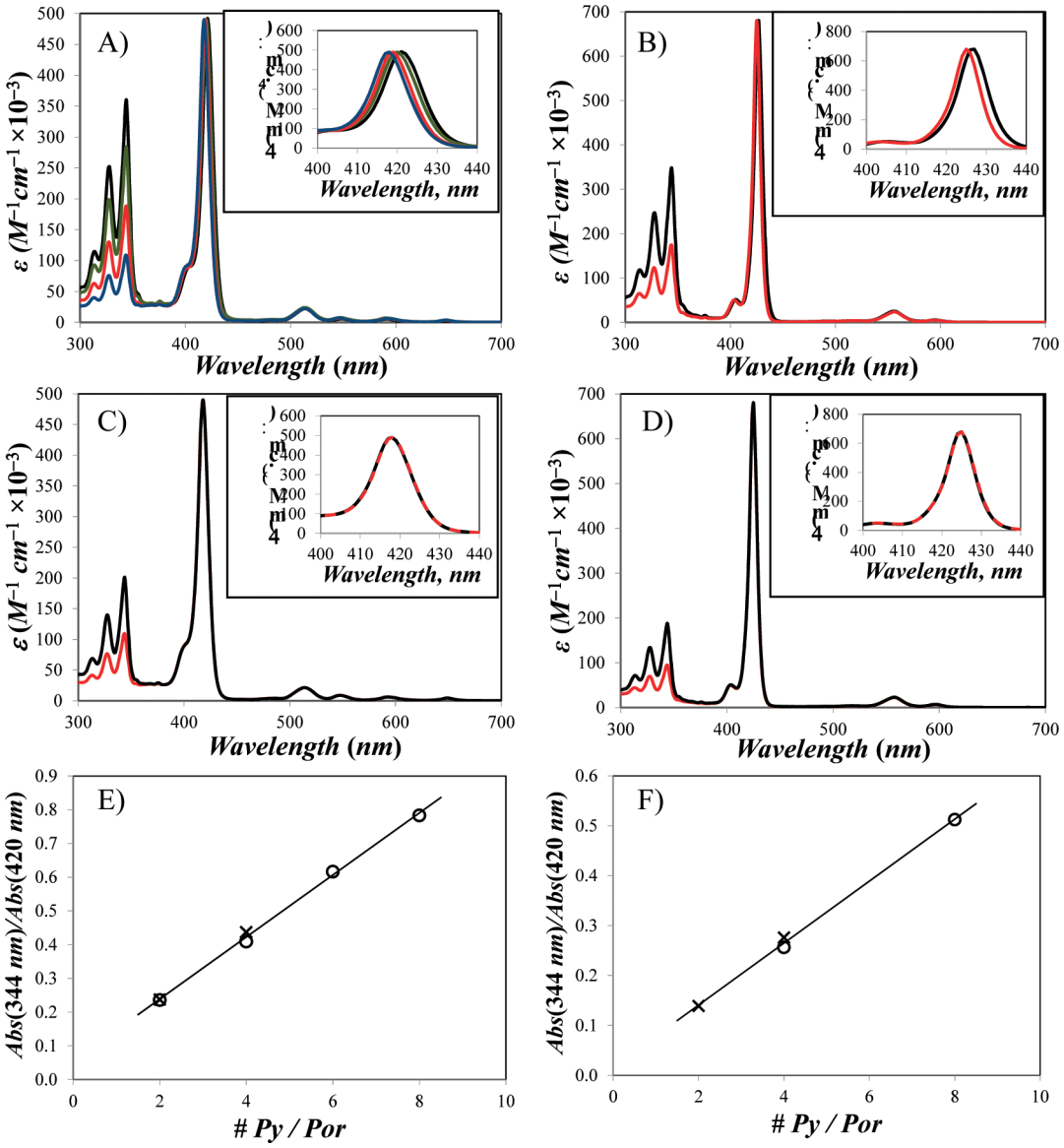

Figure 3. Absorption spectra of (A) (black —) Por-$(Py_2G1)_4$, (green —) Por-$(Py_2G1)_3$, (red —) Por-$(Py_2G1)_2$, and (blue —) Por-$(Py_2G1)_1$; (B) (black —) Zn-Por-$(Py_2G1)_4$ and (red —) Zn-Por-$(Py_2G1)_2$; (C) (black —) Por-C_4-(Py_4G2) and (red —) Por-C_4-(Py_2G1); (D) (black —) Zn-Por-C_4-(Py_4G2) and (red —) Zn-Por-C_4-(Py_2G1); and (E and F) plot of Abs(344 nm)/Abs(Soret) versus the number of pyrenyl units per porphyrinic construct for free and metalated porphyrins, respectively.

Py_2G1 and Py_4G2 dendrons. As will become clear from the MFA of the fluorescence decays acquired with all porphyrinic constructs shown in Figure 1, the impurity with the largest molar fraction is the free dendron (less than 2.6 mol %), followed by that of 1-pyrenebutanol (less than 0.042 mol %). While these molar fractions are remarkably small, the fluorescence emitted by the pyrene labels that undergo FRET with a porphyrin is so weak that even these small quantities of free-floating pyrene-labeled dendrons and pyrenebutanol can strongly affect the fluorescence spectrum of the porphyrinic constructs as their signal becomes comparable to that of the constructs shown in Figure 1.

This information was taken into account to suppress the contribution of the dendrons from the fluorescence spectra in Figure 4. Since the pyrene excimer can only be formed by the dendrons, the fluorescence spectra of the dendrons acquired in an earlier publication[21] were normalized at 480 nm, where solely the pyrene excimer emits, to the fluorescence spectra shown in Figure 4 and the normalized fluorescence spectra of the dendrons were subtracted to yield the fluorescence spectra shown in Figure 5.

The corrected fluorescence spectra in Figure 5 only show the characteristic fluorescence of the pyrene monomer and porphyrin. The fluorescence spectrum of the free porphyrin shows a single band at 650 nm for the $S_1 \rightarrow S_0$ transition in Figure 5A,B. The fluorescence spectrum of the Zn-loaded porphyrin shows a single band at 428 nm for the $S_2 \rightarrow S_0$ transition and two bands representing the $S_1 \rightarrow S_0$ transition with a main peak at 600 nm and a smaller peak at 650 nm. The pyrene monomer fluoresces with its characteristic peaks between 370 and 410 nm. The absolute fluorescence spectra of the free porphyrin TME and the Zn-loaded porphyrin TPP are also shown as dotted lines in Figure 5 for comparison. It is noticeable that in all fluorescence spectra of the porphyrinic constructs excited where pyrene absorbs, the fluorescence corresponding to the $S_1 \rightarrow S_0$ transition of porphyrin in the

dx.doi.org/10.1021/jp501445n | J. Phys. Chem. C 2014, 118, 8280−8294

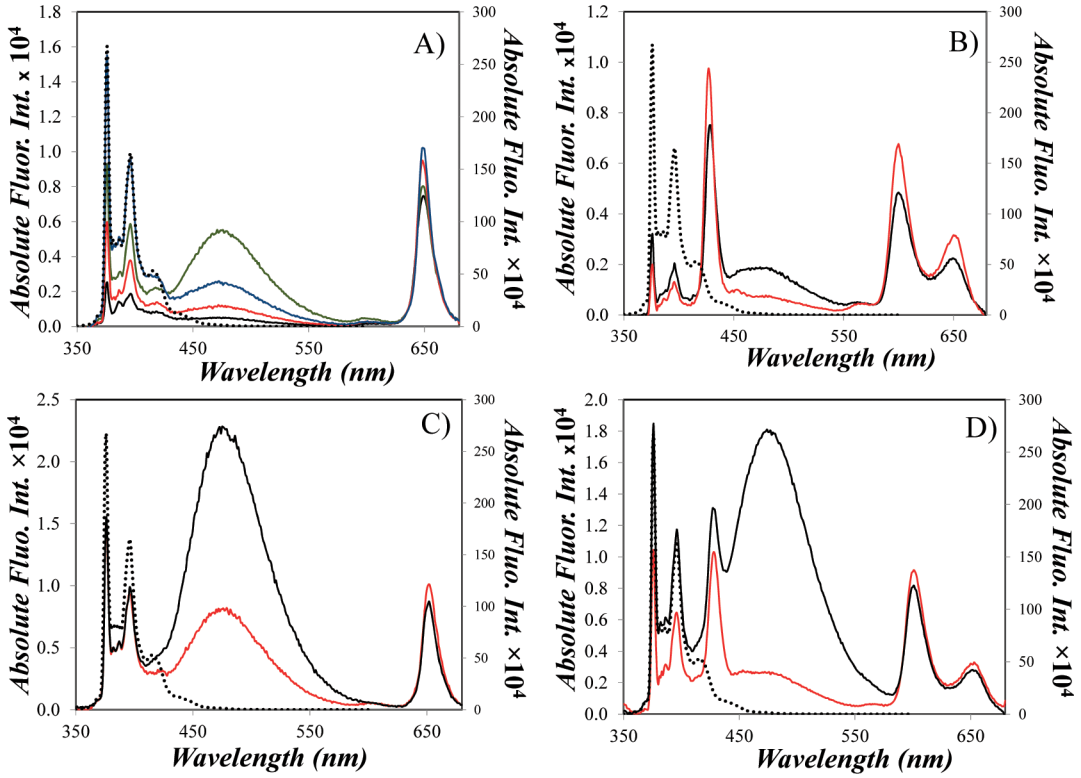

Figure 4. Spectra of the absolute fluorescence of (A) (black —) Por-$(Py_2G1)_4$, (red —) Por-$(Py_2G1)_3$, (green —) Por-$(Py_2G1)_2$, and (blue —) Por-$(Py_2G1)_1$; (B) (black —) Zn-Por-$(Py_2G1)_4$ and (red —) Zn-Por-$(Py_2G1)_2$; (C) (black —) Por-C_4-(Py_4G2) and (red —) Por-C_4-(Py_2G1); and (D) (black —) Zn-Por-C_4-(Py_4G2) and (red —) Zn-Por-C_4-(Py_2G1). The absolute fluorescence spectrum of 1-pyrenebutanol (···) is shown in all figures with its intensity reported on the secondary axis on the right-hand side.

Table 2. FRET Efficiency and d^{EXT}_{Por-Py} for Porphyrinic Constructs

	without Zn			with Zn		
sample	E_{FRET}(SS)	E_{FRET}(SPC)	d^{EXT}_{Por-Py} (Å)	E_{FRET}(SS)	E_{FRET}(SPC)	d^{EXT}_{Por-Py} (Å)
Por-$(Py_2G1)_4$	0.999	1.000	18.2	1.000	1.000	17.8
Por-$(Py_2G1)_3$	0.997	1.000	18.2			17.8
Por-$(Py_2G1)_2$	0.998	1.000	18.2	1.000	0.999	17.8
Por-$(Py_2G1)_1$	0.995	1.000	18.2			17.8
Por-C_4-(Py_2G1)	0.997	0.998	30.2	0.998	0.998	29.9
Por-C_4-(Py_4G2)	0.998	0.997	34.9	0.996	0.996	34.7

constructs has an intensity that is similar to that of the molecular porphyrin TME and Zn-TPP used in this study. This observation suggests that the energy absorbed by the pyrenyl groups is being transferred entirely to the porphyrinic core of the constructs.

The efficient FRET taking place within the constructs between an excited pyrene and a ground-state porphyrin is further confirmed by determining the quantum yield of fluorescence ϕ_{Py} and ϕ_{Por} for pyrene and porphyrin based on the fluorescence spectra shown in Figure 5. The values of ϕ_{Py} given in Table 1 reflect the efficient quenching of the 1-pyrenebutoxy label whose quantum yield is reduced by more than 200 times compared to that of 1-pyrenebutanol found to equal 0.52 in THF.[21] The ϕ_{Por} values obtained for the porphyrin constructs are very close to those measured for the free base tetramesitylporphyrin (TME) and the Zn-loaded tetraphenylporphyrin (Zn-TPP) in THF found to equal 16×10^{-4} and 30×10^{-4}, respectively. The fact that the dendronized porphyrins excited at 344 nm where pyrene absorbs strongly have a quantum yield ϕ_{Por} similar to that of the non-dendronized porphyrins suggests that all the energy absorbed by pyrene is efficiently transferred to porphyrin.

The fluorescence spectra shown in Figure 5 and the fluorescence spectrum of 1-pyrenebutanol in Figure 4 were used to determine the efficiency of FRET with eq 3 by integrating the fluorescence of the pyrene monomer between 350 and 500 nm to yield I_{Py}(porphyrinic constructs) and I_{PyBuOH}, respectively. The efficiencies E_{FRET}(SS) obtained by steady-state fluorescence for all the constructs have been reported in Table 2.

$$E_{FRET}(SS) = 1 - \frac{I_{Py}(\text{porphyrinic constructs})}{I_{PyBuOH}} \quad (3)$$

As all E_{FRET}(SS) values listed in Table 2 are close to unity, they confirm the efficient transfer of energy from an excited pyrene to a ground-state porphyrin. Ideally, E_{FRET}(SS) should be related to the fully extended distance between porphyrin and pyrene, referred to as d^{EXT}_{Por-Py}, becoming closer to unity as d^{EXT}_{Por-Py}decreases. The fully extended distance d^{EXT}_{Por-Py} was

dx.doi.org/10.1021/jp501445n | J. Phys. Chem. C 2014, 118, 8280−8294

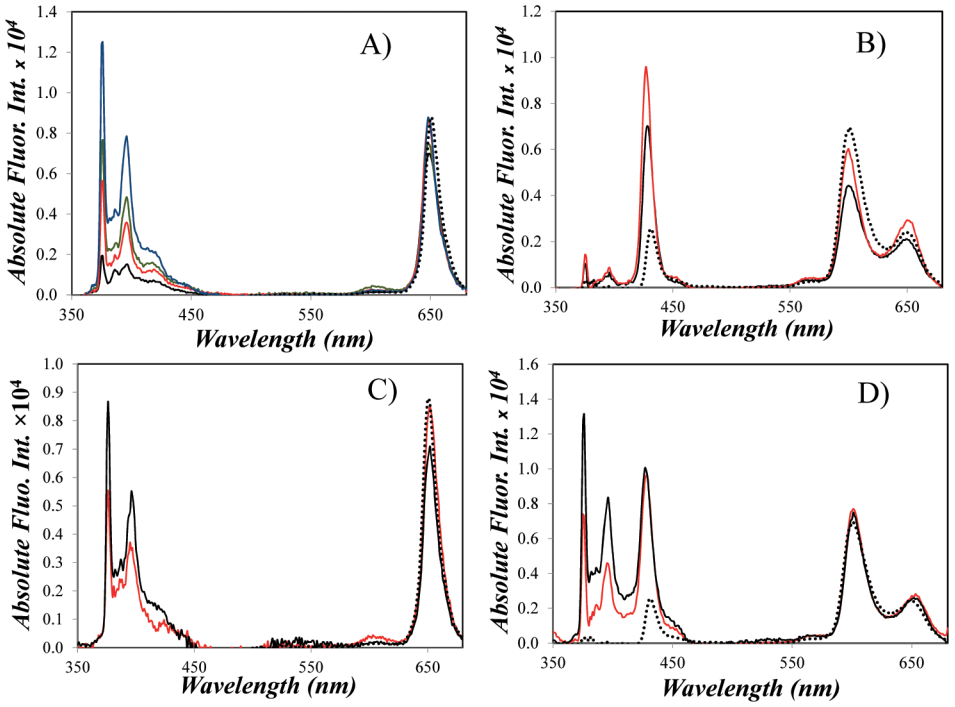

Figure 5. Spectra of the absolute fluorescence of (A) (black —) Por-$(Py_2G1)_4$, (green —) Por-$(Py_2G1)_3$, (red —) Por-$(Py_2G1)_2$, and (blue —) Por-$(Py_2G1)_1$; (B) (black —) Zn-Por-$(Py_2G1)_4$ and (red —) Zn-Por-$(Py_2G1)_2$; (C) (black —) Por-C_4-(Py_4G2) and (red —) Por-C_4-(Py_2G1); and (D) (black —) Zn-Por-C_4-(Py_4G2) and (red —) Zn-Por-C_4-(Py_2G1). The absolute fluorescence spectra of the free porphyrin TME in parts A and C and Zn-TPP in parts B and D (···) are shown.

determined by conducting molecular mechanics optimizations with the program Hyperchem. The expected relationship between E_{FRET} and d^{EXT}_{Por-Py} was observed for the Zn-loaded porphyrinic constructs in Table 2, but not for the free-base constructs for which $E_{FRET}(SS)$ varied between 0.995 and 0.999 for the constructs where the dendrons were directly attached to the base, although d^{EXT}_{Por-Py} for these constructs is the same. These discrepancies were attributed to the efficient quenching undergone by the pyrene labels, which makes the analysis of the fluorescence spectra highly sensitive to the presence of unwanted fluorescent impurities. In particular, pyrene excimer formation observed in Figure 4 for all the porphyrinic constructs has been attributed to the presence of free dendrons in the solutions. Whereas the contribution of the different chromophore species found in solution is challenging to sort out through the quantitative analysis of fluorescence spectra, this information is much easier to obtain from the analysis of fluorescence decays as each chromophore species is endowed with a specific temporal response. Consequently, the fluorescence decays of the pyrene monomer and porphyrin of all the dendronized porphyrins were acquired and fitted globally according to model free analysis (MFA).[16,17,21] MFA provides information about the time scale over which a given photophysical process, in this case FRET, takes place as well as the molar fractions of the different chromophores involved in FRET and other photophysical processes.

Analysis of Fluorescence Decays. As three photophysical phenomena can theoretically take place intramolecularly and simultaneously in the porphyrinic constructs, the analysis of the fluorescence decays is challenging. These photophysical processes have been depicted in Scheme 1. Upon excitation of the solution at 344 nm, both porphyrin and pyrene can absorb a photon. Upon absorption, the excited porphyrin will emit fluorescence with its natural lifetime τ_{Por}. The excited

Scheme 1. Photophysical Processes Taking Place in Porphyrinic Constructs, Where Dashed Arrows Indicate Unlikely Processes

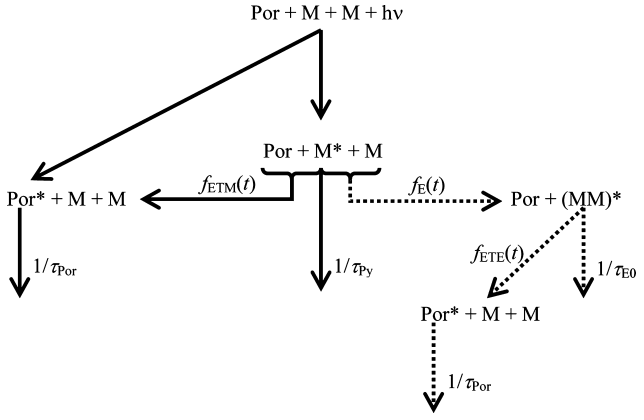

pyrene monomer can emit fluorescence with its natural lifetime τ_{Py}, form an excimer E0* with a time-dependent excimer formation "rate constant" $f_E(t)$, or undergo FRET with a time-dependent "rate constant" $f_{ETM}(t)$. The pyrene excimer can fluoresce with its natural lifetime τ_{E0} or undergo FRET to the porphyrin with a time-dependent "rate constant" $f_{ETE}(t)$. The time dependency of $f_E(t)$ comes as a result of the strong dependence of the rate constant of end-to-end cyclization of linear chains with chain length.[18] Consequently, every pyrene pair separated by a different chain length will form an excimer with a different rate constant, implying that all porphyrinic constructs having more than two pyrenes will form excimers with a distribution of rate constants, rapidly and slowly at the early and later times, respectively. The time dependency of $f_{ETM}(t)$ and $f_{ETE}(t)$ is a consequence of the Brownian motion

dx.doi.org/10.1021/jp501445n | J. Phys. Chem. C 2014, 118, 8280−8294

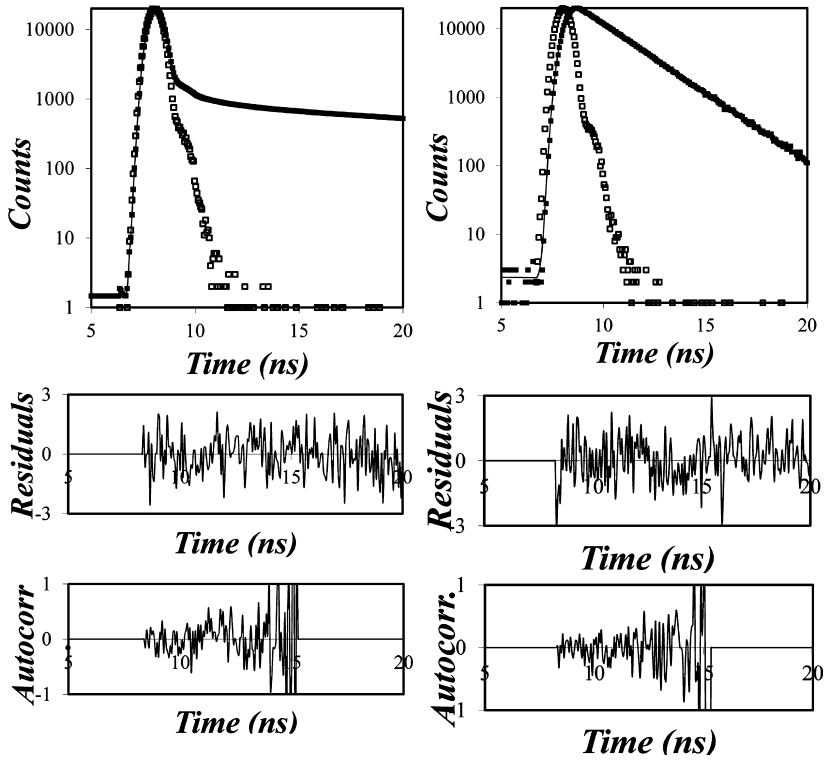

Figure 6. Pyrene (left, λ_{em} = 375 nm) and porphyrin (right, λ_{em} = 610 nm) fluorescence decays of Zn-Por-$(Py_2G1)_2$ fitted globally according to MFA. λ_{ex} = 344 nm. χ^2 = 1.01.

of the chromophoric species in solution which affects the distribution of the through-space distances (d^{TS}_{Por-Py}) between porphyrin and pyrene as a function of time. Since FRET depends strongly on the distance between the donor and acceptor, donor and acceptor (D−A) pairs separated by short distances undergo FRET first. Depletion of this population of D−A pairs is balanced by diffusion in solution that brings excited donors back within striking distance of the acceptor, thus continually replenishing the D−A pairs separated by short distances.

The handling of the photophysical processes described in Scheme 1 can be greatly facilitated by considering that excimer formation in the pyrene-labeled dendrons occurs much more slowly than FRET between an excited pyrene monomer and a ground-state porphyrin. Indeed, an earlier report established that the average rate constant of pyrene excimer formation $\langle k_E \rangle$ for the Py_2G1 and Py_4G2 dendrons equaled 3.2×10^7 and 11.2×10^7 s^{-1}, respectively.[29] Doubling the local pyrene concentration in the dendron resulted in a 3.5-fold increase in $\langle k_E \rangle$. In turn, the average rate constant for FRET between an excited pyrene and a ground-state porphyrin $\langle k_{ET} \rangle$ in the Por-C_4-(Py_2G1) and Por-C_4-(Py_4G2) constructs was found to equal 2.3×10^9 and 1.8×10^9 s^{-1}, respectively.[21] The slight decrease in $\langle k_{ET} \rangle$ from Por-C_4-(Py_2G1) to Por-C_4-(Py_4G2) reflects the increase in the value of d^{EXT}_{Por-Py} in Table 2 between the two constructs. Since $\langle k_{ET} \rangle$ was at least 16 times larger than $\langle k_E \rangle$, it was concluded that very little excimer would form in the constructs as FRET would deactivate an excited pyrene monomer before having had a chance to encounter a ground-state pyrene to form an excimer. In the case of the porphyrinic constructs having no C_4-linker between the porphyrin and the pyrene-labeled dendron, the distance d^{EXT}_{Por-Py} is much shorter, $\langle k_{ET} \rangle$ is thus much larger, and the possibility of excimer formation in these constructs can be entirely ruled out. This discussion justifies the procedure that was applied to analyze the fluorescence spectra in Figure 4 where the excimer emission was attributed solely to the presence of free dendrons.

While this insight simplified the analysis of the photophysical processes undergone by the constructs, the analysis of the fluorescence decays still needed to handle the time-dependent rate constant for FRET between the excited pyrene and a ground-state porphyrin, $f_{ETM}(t)$. While mathematical procedures have been implemented to handle quantitatively $f_{ETM}(t)$ in the case of linear peptides terminated at one end with an energy donor and at the other end with an energy acceptor,[30] no analytical method is currently capable of describing the function $f_{ETM}(t)$ quantitatively for the complex architectures of the porphyrin constructs shown in Figure 1. On the other hand, model free analysis (MFA) has been shown to provide relevant information about $\langle k_{ET} \rangle$.[21] MFA is based on the observation that any fluorescence decay can be fitted with a sum of exponentials where the decay times τ_i used in the sum of exponentials equal $(\tau_{Py}^{-1} + k_{ETi})^{-1}$ and k_{ETi} is one element of the distribution of rate constants describing FRET. Since quenching of an excited pyrene monomer by FRET with a rate constant k_{ETi} results in the generation of an excited porphyrin with the same rate constant, the decay times τ_i were set to be the same in the global analysis of the pyrene and porphyrin decays. Furthermore, the pre-exponential factors in eq S2 in the Supporting Information were also optimized as a function of the τ_i decay times as is typically done by the Duhamel laboratory.[10,16,17]

As shown in Figure 6 where MFA was applied to the pyrene and porphyrin decays of Zn-Por-$(Py_2G1)_2$, MFA of the pyrene monomer and porphyrin fluorescence decays indicated that FRET in the constructs where the dendrons were directly attached to the porphyrin occurred extremely rapidly with a decay time of 64 ± 11 ps. Considering that the shortest time

dx.doi.org/10.1021/jp501445n | J. Phys. Chem. C 2014, 118, 8280−8294

Table 3. Pre-Exponential Factors and Decay Times Retrieved from Global Model Free Analysis of Pyrene Monomer Decays for (A) Free and (B) Metalated Porphyrin Constructs in THF[a]

(A)									
sample	τ_1 (ns)	a_1	τ_2 (ns)	a_2	τ_3 (ns)	a_3	${}^{F}f_{Mden}$	${}^{F}f_{Mfree}$	χ^2
Por-$(Py_2G1)_4$	0.067	0.991	2.3	0.006			0.003	0.000	1.25
Por-$(Py_2G1)_3$	0.054	0.997	3.4	0.001			0.002	0.000	1.15
Por-$(Py_2G1)_2$	0.055	0.998	2.4	0.001			0.002	0.000	1.04
Por-$(Py_2G1)_1$	0.066	0.992	5.1	0.006			0.002	0.001	1.14
Por-C_4-(Py_2G1)	0.21	0.11	0.45	0.54	3.2	0.01	0.01	0.00	1.07
Por-C_4-(Py_4G2)	0.22	0.42	0.72	0.55	3.0	0.01	0.03	0.00	1.16
(B)									
sample	τ_1 (ns)	a_1	τ_2 (ns)	a_2	$\tau_3{}^{b}$ (ns)	$a_3{}^{b}$	${}^{F}f_{Mden}$	${}^{F}f_{Mfree}$	χ^2
Zn-Por-$(Py_2G1)_4$	0.083	0.953	1.5	0.026			0.021	0.000	1.23
Zn-Por-$(Py_2G1)_2$	0.061	0.993					0.004	0.000	1.01
Zn-Por-C_4-(Py_2G1)	0.22	0.49	0.54	0.48	3.3	0.02	0.01	0.00	0.96
Zn-Por-C_4-(Py_4G2)	0.09	0.27	0.81	0.68	2.0	0.01	0.03	0.00	1.05

[a]In eq S1 in the Supporting Information used to fit the pyrene monomer fluorescence decay, the lifetime τ_{Py} was fixed at 190 ns and using the function $f_{den}(t)$ = 0.78 exp(−t/17.4 ns) + 0.22 exp(−t/54.9 ns) for Py_2G1 and $f_{den}(t)$ = 0.52 exp(−t/5.1 ns) + 0.43 exp(−t/7.4 ns)+ 0.05 exp(−t/48 ns) for Py_4G2. [b]The decay time τ_3 is not coupled with the porphyrin decay, and it is not included in the calculation of $\langle k_{ET} \rangle$. It represents residual FRET from the excited pyrene to the S_2 excited state of the porphyrin.

Table 4. Pre-Exponential Factors and Decay Times Retrieved from Global Model Free Analysis of Porphyrin Decays for (A) Free and (B) Metalated Porphyrin Constructs in THF[a]

(A)								
sample	τ_{Por1} (ns)	${}^{F}f_{ET}^{Por1}$	${}^{F}f_{Por1}$	τ_{Por2} (ns)	${}^{F}f_{ET}^{Por2}$	${}^{F}f_{Por2}$	${}^{F}f_{exci}$	χ^2
Por-$(Py_2G1)_4$	8.3	0.44	0.05	11.9	0.47	0.01	0.02	1.25
Por-$(Py_2G1)_3$	12.8	0.45	0.09	11.9	0.45	0.00	0.01	1.15
Por-$(Py_2G1)_2$	11.4	0.02	0.13	11.9	0.83	0.00	0.02	1.04
Por-$(Py_2G1)_1$	6.0	0.12	0.00	11.9	0.63	0.22	0.02	1.14
Por-C_4-(Py_2G1)	8.7	0.09	0.01	11.9	0.66	0.22	0.03	1.07
Por-C_4-(Py_4G2)	12.5	0.38	0.13	11.9	0.49	0.00	0.00	1.16
(B)								
sample	τ_{Por1} (ns)	${}^{F}f_{ET}^{Por1}$	${}^{F}f_{Por1}$	τ_{Por2} (ns)	${}^{F}f_{ET}^{Por2}$	${}^{F}f_{Por2}$	${}^{F}f_{exci}$	χ^2
Zn-Por-$(Py_2G1)_4$	1.5	0.80	0.03	2.1	0.17	0.00	0.00	1.23
Zn-Por-$(Py_2G1)_2$	2.2	0.26	0.06	2.1	0.68	0.00	0.00	1.01
Zn-Por-C_4-(Py_2G1)	2.2	0.89	0.11				0.00	0.96
Zn-Por-C_4-(Py_4G2)	2.2	0.94	0.06				0.00	1.05

[a]In eq S2 in the Supporting Information used to fit the porphyrin decays, the lifetimes τ_M and τ_{E0} were fixed at 190 and 47 ns for the pyrene monomer and excimer, respectively. The lifetime of Por2* was fixed at the long lifetime 11.9 or 2.1 ns of the porphyrinic constructs excited at 365 nm.

per channel accessible with the time-resolved fluorometer used in this study equaled 59 ps/channel, implying that the signal due to FRET for these constructs had vanished after five channels, a number of precautions were taken for the analysis of the fluorescence decays.

First, the fluorescence decays of the pyrene monomer and porphyrin were fitted globally making sure that the decay time in the monomer decay due to FRET would be matched by an equivalent rise time in the porphyrin decay. Second, all parameters that could be determined through separate control experiments were fixed in the analysis. These included the contribution from the free dendrons ($f_{den}(t)$ in eq S1 in the Supporting Information) to the pyrene monomer decays, the natural lifetime of the pyrene monomer (τ_{Py} = 190 ns for 1-pyrenebutanol in THF), the pyrene excimer natural lifetime (τ_{E0} = 47 ns) contributing to the porphyrin decay which was found by acquiring a fluorescence decay at 510 nm where only the pyrene excimer emits, and the long lifetimes used for the porphyrins (τ_{Por} = 11.9 ns and $\tau_{Zn\text{-}Por}$ = 2.1 ns for the free and Zn-loaded prophyrin, respectively) which were obtained from fitting the fluorescence decays of TME and Zn-TPP in THF. Third, the ratio of the absorbance at 344 nm due to the pyrene labels over that due to the porphyrin, namely, the ratio in eq 4, was fixed in the analysis where n was changed from 8 to 2 depending on the specific pyrene content of the constructs.

$$\text{ratio} = \frac{n\varepsilon_{Py}(344\text{ nm})([Py_{ET}]_{t=0}^{Por1*} + [Py_{ET}]_{t=0}^{Por2*})}{\varepsilon_{Por}(344\text{ nm})([Por1]_{t=0} + [Por2]_{t=0})} \quad (4)$$

Implementation of these additional constraints in the analysis program led to a set of parameters that provided a meaningful description of the photophysics undergone between pyrene and porphyrin. The analysis did not account for the Zn-loaded porphyrins undergoing an $S_2 \rightarrow S_0$ transition as this process occurs with a decay time of ∼1.5 ps,[31] much too fast to be detected with the time-resolved fluorometer that could handle a time per channel no shorter than 59 ps/channel. The analysis did however find an uncoupled decay time of ∼2−3 ns for the fluorescence decay of pyrene in the metalated Zn-Por-C_4-

dx.doi.org/10.1021/jp501445n | J. Phys. Chem. C 2014, 118, 8280−8294

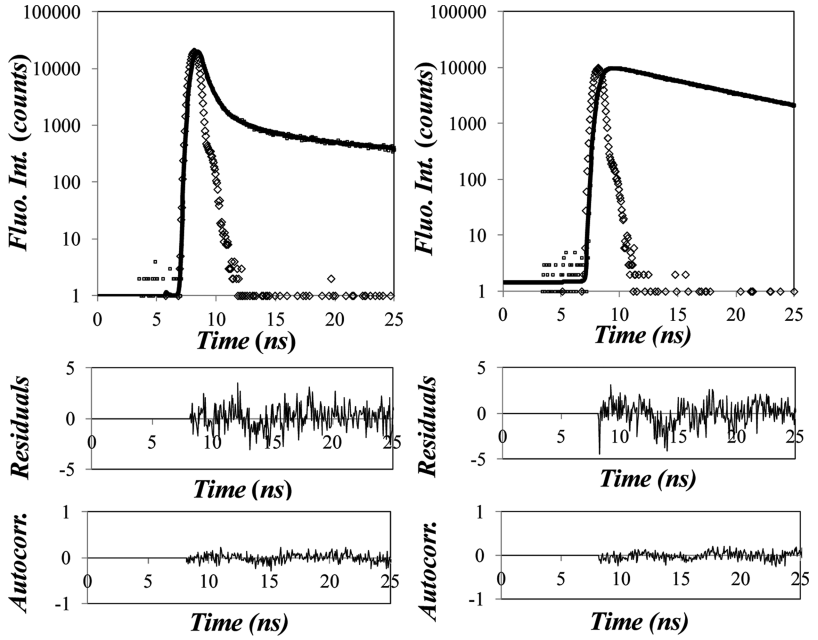

Figure 7. Pyrene (left, λ_{em} = 375 nm) and porphyrin (right, λ_{em} = 610 nm) fluorescence decays of Por-C_4-(Py_4G2) fitted globally according to MFA. λ_{ex} = 344 nm. χ^2 = 1.16.

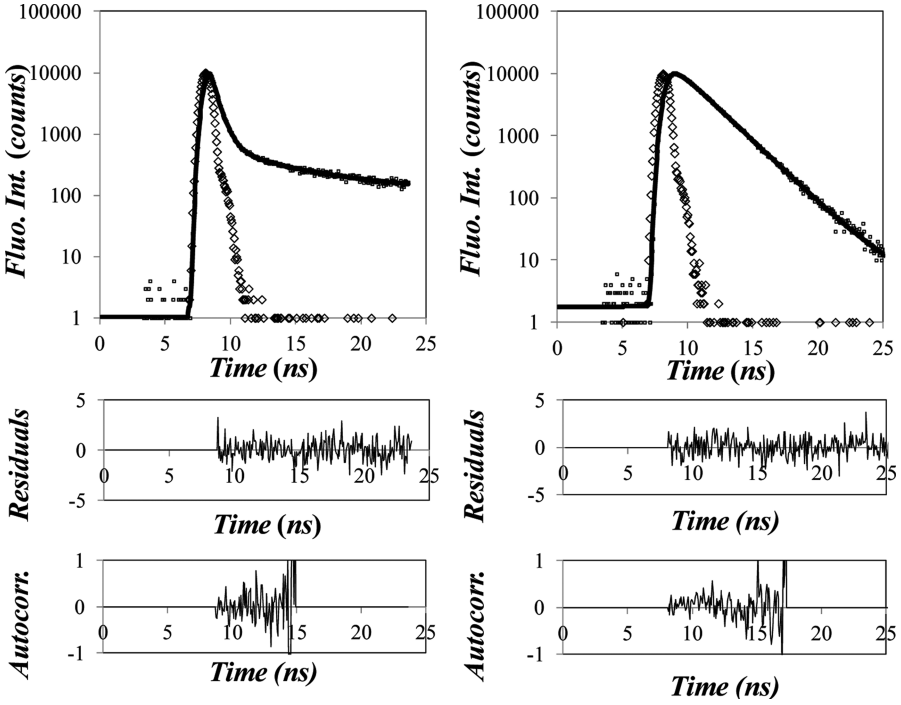

Figure 8. Pyrene (left, λ_{em} = 375 nm) and porphyrin (right, λ_{em} = 610 nm) fluorescence decays of Zn-Por-C_4-(Py_4G2) fitted globally according to MFA. λ_{ex} = 344 nm. χ^2 = 1.05.

(Py_2G1) and Zn-Por-C_4-(Py_4G2) constructs which was attributed to FRET from an excited pyrene to the S_2 electronic level of the metalated porphyrin. The contribution for this photophysical process was found to be small with a pre-exponential factor a_3 < 0.02 in Table 3B.

Global analysis of the fluorescence decays of the pyrene monomer and porphyrin yielded good fits with χ^2 values smaller than 1.30 and residuals and autocorrelation of residuals randomly distributed around zero. The parameters retrieved from the analysis are provided in Tables 3 and 4. We refer to the fractions ^{F}f used in Tables 3 and 4 and Tables S2 and S3 in the Supporting Information to represent the contribution to the fluorescence decay of one chromophore species. The fractions ^{F}f and molar fractions of the different species present in solution are listed in Tables S2 and S3 in the Supporting Information.

In addition to the fits shown in Figure 6 for Zn-Por-(Py2G1)$_2$, the fits of Por-C_4-(Py_4G2) and Zn-Por-C_4-(Py_4G2) are shown in Figures 7 and 8. Comparison of the pyrene monomer fluorescence decays shown in the left panels of

dx.doi.org/10.1021/jp501445n | J. Phys. Chem. C 2014, 118, 8280−8294

Figures 6 and 8 clearly demonstrates the effect that d^{EXT}_{Por-Py} has on FRET. Whereas the pyrene monomer decay of Zn-Por-$(Py_2G1)_2$ is undistinguishable from the instrument response function at the early times describing the FRET process in Figure 6, it is well-resolved in Figure 8 for the Zn-Por-C_4-(Py_4G2) construct where pyrene and porphyrin are separated by a larger d^{EXT}_{Por-Py} distance (see Table 2). On the other hand, metalation of the porphyrin does not seem to affect FRET as similar pyrene monomer decays are obtained in Figures 7 and 8 for the base-free Por-C_4-(Py_4G2) and metalated Zn-Por-C_4-(Py_4G2) constructs.

While the fluorescence decay of the pyrene monomer is largely unaffected by the presence of Zn in the porphyrin, the Zn-loaded porphyrin decays much more quickly in the right panel of Figure 8 with a lifetime of 2.1 ns than the free base which decays with a lifetime of 11.9 ns in the right panel of Figure 7. Since the presence of Zn does not affect much the center-to-center distance d^{EXT}_{Por-Py} and the Förster radius R_o (see Tables 1 and 2), FRET from the excited pyrene monomer to the ground-state porphyrin occurs with a similar efficiency resulting in similar pyrene monomer decays.

The coupled decay times τ_i and the normalized pre-exponential factors a_i retrieved from the global MFA of the fluorescence decays with eqs S1 and S2 in the Supporting Information were used to calculate the average rate constant for FRET $\langle k_{ET}\rangle$ between an excited pyrene monomer and ground-state porphyrin according to eq 5.

$$\langle k_{ET}\rangle = \frac{1}{\langle\tau\rangle} - \frac{1}{\tau^{\circ}_{Py}} \tag{5}$$

In eq 5, $\langle\tau\rangle$ is the average lifetime of the pyrene monomer given by $\langle\tau\rangle = \sum_{i=1}^{n} a_i\tau_i$, where the pre-exponential factors a_i have been normalized to unity. Not surprisingly, the average rate constant $\langle k_{ET}\rangle$ for FRET was found to take similar values equal to 2.2×10^9 and 2.6×10^9 s^{-1} for Por-C_4-(Py_4G2) and Zn-Por-C_4-(Py_4G2), respectively.

The $\langle k_{ET}\rangle$ values obtained with all the constructs have been listed in Table 5. Although some uncertainty might be expected from MFA of the fluorescence decays acquired with the porphyrinic constructs with no linker due to the very efficient FRET process occurring on a same time scale as the shortest time per channel of the time-resolved fluorometer, the $\langle k_{ET}\rangle$ values that were obtained from this analysis were consistent with each other. With a $\langle k_{ET}\rangle$ value of 14 ($\pm$3) $\times 10^9$ s^{-1}, FRET occurred 6 times more quickly in the constructs without C_4-linker than in the constructs Por-C_4-(Py_2G1) and Zn-Por-C_4-(Py_2G1). This large increase in $\langle k_{ET}\rangle$ is due to the shorter d^{EXT}_{Por-Py} distance of the Por-$(Py_2G1)_x$ constructs given in Table 5. It also agrees with the FRET efficiencies close to unity found for these constructs in Table 2.

Table 5. Average Rate Constant $\langle k_{ET}\rangle$ for FRET and d^{TS}_{Por-Py} in the Constructs

	without Zn		with Zn	
sample	$\langle k_{ET}\rangle$ (10^9 s^{-1})	d^{TS}_{Por-Py} (Å)	$\langle k_{ET}\rangle$ (10^9 s^{-1})	d^{TS}_{Por-Py} (Å)
Por-$(Py_2G1)_4$	12.2	14.2	12.0	13.4
Por-$(Py_2G1)_3$	17.2	13.4		
Por-$(Py_2G1)_2$	17.7	13.4	16.4	12.7
Por-$(Py_2G1)_1$	10.6	14.6		
Por-C_4-(Py_2G1)	2.2	18.9	2.6	17.3
Por-C_4-(Py_4G2)	1.9	19.4	1.7	18.7

Furthermore, $\langle k_{ET}\rangle$ could also be used to determine the FRET efficiency referred to E_{FRET}(SPC) to emphasize that it was obtained through the analysis of the fluorescence decays. This was accomplished by using eq 6. The E_{FRET}(SPC) values retrieved from using eq 6 are listed in Table 2. As for the E_{FRET}(SS) values, they are close to unity, reflecting the efficient FRET process between pyrene and porphyrin. Most importantly, E_{FRET}(SPC) values followed the expected trend with d^{EXT}_{Por-Py}, showing a continuous decrease in E_{FRET}(SPC) with increasing d^{EXT}_{Por-Py}. The nice correlation observed between E_{FRET}(SPC) and d^{EXT}_{Por-Py} is believed to result from the ability of MFA to isolate with great accuracy the contribution originating from FRET in the fluorescence decays.

$$E_{FRET}(SPC) = \frac{\tau_{Py}\langle k_{ET}\rangle}{1 + \tau_{Py}\langle k_{ET}\rangle} \tag{6}$$

The average through-space distance d^{TS}_{Por-Py} separating the pyrene monomer from the porphyrin core in the constructs could be estimated by using eq 7, which relates $\langle k_{ET}\rangle$ to d^{TS}_{Por-Py}.

$$\langle k_{ET}\rangle = \frac{1}{\tau^{\circ}_{Py}}\left(\frac{R_o}{d^{TS}_{Por-Py}}\right)^6 \tag{7}$$

The resulting d^{TS}_{Por-Py} values are listed in Table 5. As the center-to-center distance d^{EXT}_{Por-Py} of the fully stretched constructs increased from 18 to 35 Å in Table 2 for the different constructs, d^{TS}_{Por-Py} increased from 14 $\pm$ 1 to 19.0 $\pm$ 0.4 Å in Table 5, indicating that d^{TS}_{Por-Py} is always smaller than d^{EXT}_{Por-Py}. As a matter of fact, plotting d^{TS}_{Por-Py} as a function of d^{EXT}_{Por-Py}, where the distances have been expressed in angstroms as done in Figure 9, shows that d_{FRET} scales as $3.0(d^{EXT}_{Por-Py})^{0.5}$.

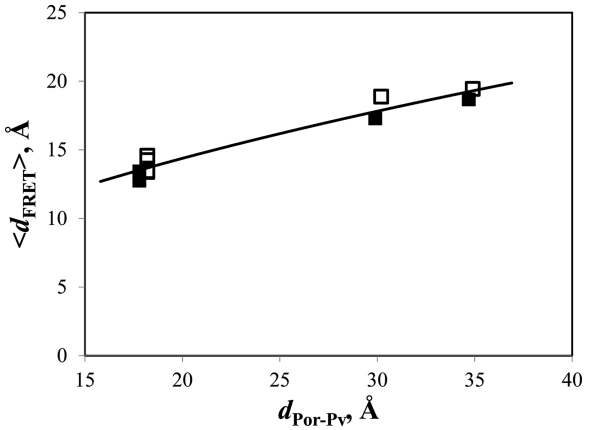

Figure 9. Plot of d^{TS}_{Por-Py} as a function of d^{EXT}_{Por-Py} for porphyrinic constructs (□) without and (■) with Zn. $d^{TS}_{Por-Py} = 3.0(d^{EXT}_{Por-Py})^{0.5}$, with both distances expressed in angstroms.

Interestingly, a scaling exponent of 0.5 would be expected if the porphyrin and pyrene monomer were separated by a chain made of freely jointed segments.

Since the end-to-end distance of a freely jointed linear chain would equal $N_K^{0.5}l_K$, where N_K and l_K are the number and length of the Kuhn segments, the relationship $d^{TS}_{Por-Py} = l_K N_K^{0.5} = 3.0(d^{EXT}_{Por-Py})^{0.5}$ obtained in Figure 9 suggests that the Kuhn length l_K for the linker spanning porphyrin and pyrene equals 9 Å since d^{EXT}_{Por-Py} equals $N_K l_K$. If this is the case, the spacer in the

dx.doi.org/10.1021/jp501445n | J. Phys. Chem. C 2014, 118, 8280−8294

constructs Por-$(Py_2G1)_1$ and Por-C_4-(Py_4G2) separating the porphyrin and the pyrene monomer with d^{EXT}_{Por-Py} distances equal to 18.2 and 34.9 Å would be equivalent to two and four Kuhn segments, respectively.

Due to the small number of Kuhn segments, the polyether spacers separating the porphyrin and the pyrene moieties are expected to be relatively stiff, which will reduce diffusive motion, a conclusion that is supported by the presence of the rigid aryl units in the spacer. As a matter of fact, the flexibility of the polyaryl backbone of the Fréchet type Py_2G1 and Py_4G2 dendrons has been probed by applying MFA to describe the process of pyrene excimer formation.[29] This study led to the conclusion that the polyaryl backbone was much stiffer than that of dendrons of a similar generation prepared with a flexible bis(hydroxymethyl)propionic acid backbone. The relatively rigid backbone separating the porphyrin from the pyrene monomer is not expected to affect as much FRET which depends on the through-space distance between the two chromophores as it does pyrene excimer formation since an excimer is formed upon contact between the two pyrene moieties whose diffusion is hindered by the backbone.

The high local concentration of chromophoric species present in the porphyrinic constructs would be expected to lead to some level of association via $\pi-\pi$ interactions. However, none of the spectroscopic data obtained so far suggest chromophore association. First, the absorption spectra of the porphyrinic constructs appear to be the sum of the individual absorption spectra of pyrene and porphyrin as supported by the straight lines obtained in Figure 3E,F. Second, and most importantly, the rise time in the porphyrin decay matches perfectly the decay time in the pyrene monomer decay and the pre-exponential factors obey the relationship expected from their respective molar absorbance coefficient and the chemical composition of the porphyrinic construct. Such a good agreement would not be obtained if ground-state complexes between porphyrin and pyrene were generated in solution. We note that the existence of ground-state pyrene aggregates can be safely ruled out since they have been shown to be absent from the pyrene-labeled dendrons in THF.[21]

CONCLUSIONS

A series of six different constructs with a single porphyrin at the core and pyrenes at the periphery were prepared. Porphyrin and pyrene were selected as they act as excellent FRET acceptor and donor, respectively. To enhance the ability of the constructs to capture light at 344 nm, the number of pyrene units was increased from two to eight by taking advantage of the use of pyrene end-labeled dendrons of generation 1 (Py_2G1) and generation 2 (Py_4G2) and the possibility of labeling the porphyrin core at all four meso positions. All spectroscopic data indicated that the excitation energy remained localized on the invidual pyrene or porphyrin chromophores and that the energy was transferred effectively from an excited peripheral pyrene to the porphyrin core of the constructs. As a result, the number of pyrenes did not affect the FRET process, but an increasing number of pyrenes led to a more efficient light collection per construct due to the corresponding increase in the molar absorbance coefficient at 344 nm where pyrene absorbs.

While the number of pyrene groups present in a given construct did not affect FRET efficiency, the FRET efficiency could be tuned efficiently by adjusting the number of bonds separating porphyrin from pyrene. The shortest chain length of 18.2 Å separating porphyrin from pyrene was obtained with the Por-$(Py_2G1)_x$ series, where the Py_2G1 dendrons were covalently attached directly onto the porphyrin. Using a C_4-butanoate linker between the porphyrin core and the Py_2G1 linker provided an intermediate separation distance of 30.2 Å between porphyrin and pyrene. Using a Py_4G2 dendron where the pyrene end groups were separated by a longer chain from the dendron focal point afforded a separation length of 34.9 Å between porphyrin and pyrene. These separation distances referred to as d^{EXT}_{Por-Py} in Table 2 led to differences in FRET that could be nicely accounted for in the global MFA of the pyrene and porphyrin fluorescence decays. The average rate constant for FRET, $\langle k_{ET} \rangle$ in Table 5, and the FRET efficiency, E_{FRET}(SPC) in Table 2, decreased continuously with increasing d^{EXT}_{Por-Py} as expected from the relationship given in eq 7 relating k_{ET} and the through-space distance separating the donor from the acceptor. While the analysis of the fluorescence spectra confirmed the efficient intramolecular FRET from an excited pyrene to a ground-state porphyrin located in the same construct yielding an E_{FRET}(SS) close to unity, E_{FRET}(SS) did not show a continuous decrease with increasing d_{Por-Py} contrary to what would be theoretically expected. This discrepancy was attributed to the efficient FRET which made difficult the quantitative analysis of the steady-state fluorescence spectra, as the fluorescence signal of residual fluorescent impurities such as free 1-pyrenebutoxy labels or free pyrene end-labeled dendrons competed with the extremely weak fluorescence emitted by the dendronized porphyrins. This complication was successfully circumvented by fitting the fluorescence decays of the pyrene donor and porphyrin acceptor globally according to MFA. Comparison of the fluorescence decay times that were coupled in the fluorescence decays of the pyrene monomer and porphyrin provided clear evidence that these decay times were involved in FRET. Taking the stringent precautions described in this paper to apply MFA, the MFA of the fluorescence decays yielded the contributions of all the chromophores present in the solution, as well as the time scale over which FRET occurred. The main effect of metalating the porphyrins with Zn was to shorten the porphyrin lifetime from 11.9 to 2.1 ns as shown in Figures 7 and 8. The Zn-loaded porphyrins yielded similar E_{FRET} and $\langle k_{ET} \rangle$ values as expected from the similar R_o and d^{EXT}_{Por-Py} values obtained for both the free and Zn-loaded porphyrins.

The through-space distance d^{TS}_{Por-Py} separating the donor and acceptor obtained from the analysis of the $\langle k_{ET} \rangle$ values according to eq 7 was found to scale as $3.0(d^{EXT}_{Por-Py})^{0.5}$. This relationship is interesting as it suggests that the linker separating porphyrin and pyrene can be viewed as a chain made of a number N_K of Kuhn segments of length l_K equal to 9 Å. If confirmed by other studies, it would provide an easy analytical tool to predict E_{FRET} for a given light-harvesting construct constituted of a peripheral energy donor and an energy acceptor at its core. Together, the results presented in this study provide a self-consistent set of parameters that describe quantitatively the complex FRET process undergone in these dendronized porphyrinic constructs.

ASSOCIATED CONTENT

Supporting Information

^{1}H NMR spectra of selected compounds; analysis of fluoresence decays according to MFA; molar absorption coefficients at 344 nm; molar fractions of chromophores.

dx.doi.org/10.1021/jp501445n | J. Phys. Chem. C 2014, 118, 8280−8294

This material is available free of charge via the Internet at http://pubs.acs.org.

AUTHOR INFORMATION

Notes

The authors declare no competing financial interest.

ACKNOWLEDGMENTS

We thank Miguel Canseco and Gerardo Cedillo for their help recording FTIR and NMR spectra. E.R. and G.Z.-G. are grateful to CONACYT (Project 128788) for financial support. M.F. and J.D. are thankful to NSERC for generous support of this research. R.R. and N.S. are grateful to CNRS for research funding.

REFERENCES

(1) Hu, X.; Damjanovic, A.; Ritz, T.; Schulten, K. Architecture and Mechanism of the Light-Harvesting Apparatus of Purple Bacteria. *Proc. Natl. Acad. Sci. U.S.A.* **1998**, *95*, 5935−5941.

(2) Adronov, A.; Fréchet, J. M. J. Light-Harvesting Dendrimers. *Chem. Commun.* **2000**, 1701−1710.

(3) Ceroni, P.; Bergamini, G.; Marchioni, F.; Balzani, V. Luminiscence as a Tool to Investigate Dendrimer Properties. *Prog. Polym. Sci.* **2005**, *30*, 453−473.

(4) D'Ambruoso, G. D.; McGrath, D. V. Energy Harvesting in Synthetic Dendrimer Materials. *Adv. Polym. Sci.* **2008**, *214*, 87−147.

(5) Pawlicki, M.; Collins, H. A.; Denning, R. G.; Anderson, H. L. Two-Photon Absorption and the Design of Two-Photon Dyes. *Angew. Chem., Int. Ed.* **2009**, *48*, 3244−3266.

(6) Anderson, H. L. Building Molecular Wires from the Colors of Life: Conjugated Porphyrin Oligomers. *Chem. Commun.* **1999**, 2323−2330.

(7) Gebbink, R. J.; Suijkerbuijk, B. J. Merging Porphyrins with Organometallics: Synthesis and Applications. *Angew. Chem., Int. Ed.* **2008**, *47*, 7396−7421.

(8) Senge, M. O.; Fazekas, M.; Notaras, E. G.; Blau, W. J.; Zawadzka, M.; Locos, O. B.; Mhuircheartaigh, E. N. Nonlinear Optical Properties of Porphyrins. *Adv. Mater.* **2007**, *19*, 2737−2774.

(9) Winnik, F. M. Photophysics of Preassociated Pyrenes in Aqueous Polymer Solutions and in Other Organized Media. *Chem. Rev.* **1993**, *93*, 587−614.

(10) Duhamel, J. Internal Dynamics of Dendritic Molecules Probed by Pyrene Excimer Formation. *Polymers* **2012**, *4*, 211−239.

(11) Xu, Y.; Bai, H.; Lu, G.; Li, C.; Shi, G. Flexible Graphene Films via the Filtration of Water-Soluble Noncovalent Functionalized Graphene Sheets. *J. Am. Chem. Soc.* **2008**, *130*, 5856−5857.

(12) Lee, D. W.; Kim, T.; Lee, M. An Amphiphilic Pyrene Sheet for Selective Functionalization of Graphene. *Chem. Commun.* **2011**, *47*, 8259−8261.

(13) Liu, Z.; Liu, J.; Cui, L.; Wang, R.; Luo, X.; Marrow, C. J.; Yang, W. Preparation of Graphene/Polymer Composites by Direct Exfolation of Graphite in Functionalised Block Copolymer Matrix. *Carbon* **2013**, *51*, 148−155.

(14) Wurl, A.; Goossen, S.; Canevet, D.; Sallé, M.; Pérez, E. M.; Klinke, C. Supramolecular Interaction of Single-Walled Carbon Nanotubes with a Probed by Field-Effect Transistor Devices. *J. Phys. Chem. C* **2012**, *116*, 20062−20066.

(15) Bahun, J. G.; Adronov, A. Interactions of Carbon Nanotubes with Pyrene-Functionalized Linear-Dendritic Hybrid Polymers. *J. Polym. Sci., Part A: Polym. Chem.* **2010**, *48*, 1016−1028.

(16) Duhamel, J. New Insights in the Study of Pyrene Excimer Fluorescence to Characterize Macromolecules and their Supramolecular Assemblies in Solution. *Langmuir* **2012**, *28*, 6527−6538.

(17) Duhamel, J. Global Analysis of Fluorescence Decays to Probe the Internal Dynamics of Fluorescently Labeled Macromolecules. *Langmuir* **2014**, *30*, 2307−2324.

(18) Winnik, M. A. End-to-End Cyclization of Polymer Chains. *Acc. Chem. Res.* **1985**, *18*, 73−79.

(19) Duhamel, J. Polymer Chain Dynamics in Solution Probed with a Fluorescence Blob Model. *Acc. Chem. Res.* **2006**, *39*, 953−960.

(20) Yip, J.; Duhamel, J.; Bahun, G. J.; Adronov, A. A Study of the Branch Ends of a Series of Pyrene-Labeled Dendrimers Based on Pyrene Excimer Formation. *J. Phys. Chem. B* **2010**, *114*, 10254−10265.

(21) Zaragoza-Galán, G.; Fowler, M. A.; Duhamel, J.; Rein, R.; Solladié, N.; Rivera, E. Synthesis and Characterization of Novel Pyrene-Dendronized Porphyrins Exhibiting Efficient Fluorescence Resonance Energy Transfer: Optical and Photophysical Properties. *Langmuir* **2012**, *28*, 11195−11205.

(22) Press, W. H.; Flannery, B. P.; Teukolsky, S. A.; Vetterling, W. T. *Numerical Recipes. The Art of Scientific Computing (Fortran Version)*; Cambridge University Press: Cambridge, U.K., 1992.

(23) Lakowicz, J. R. *Principles of Fluorescence Spectroscopy*; Plenum Press: New York, 1983.

(24) Lindsey, J. S.; Schreiman, I. C.; Hsu, H. C.; Margueretazz, A. M. Rothemund and Adler-Longo Reactions Revisited: Synthesis of Tetraphenylporphyrins Under Equilibrium Conditions. *J. Org. Chem.* **1987**, *52*, 827−836.

(25) Rothemund, P. A New Porphyrin Synthesis. The Synthesis of Porphyrin. *J. Am. Chem. Soc.* **1936**, *58*, 625−627.

(26) Alder, A.; Longo, F. R.; Finarelli, J. D.; Goldmacher, J.; Assour, J.; Korsakoff, L. A Simplified Synthesis for Meso-Tetraphenylporphyrine. *J. Org. Chem.* **1967**, *32*, 476.

(27) Solladié, N.; Hamel, A.; Gross, M. Synthesis of Multiporphyrinic α-Polypeptides: Towards the Study of the Migration of an Excited State for the Mimicking of the Natural Light Harvesting Device. *Tetrahedron Lett.* **2000**, *41*, 6075−6078.

(28) Valicsek, Z.; Horváth, O. Application of the Electronic Spectra of Porphyrins for Analytical Purposes: The Effects of Metal Ions and Structural Distortions. *Microchem. J.* **2013**, *107*, 47−62.

(29) Fowler, M. A.; Duhamel, J.; Bahun, G. J.; Adronov, A.; Zaragoza-Galán, G.; Rivera, E. Studying Pyrene-Labeled Macromolecules with the Model Free Analysis. *J. Phys. Chem. B* **2012**, *116*, 14689−14699.

(30) Jacob, M. H.; Dsouza, R. N.; Ghosh, I.; Norouzy, A.; Schwazlose, T.; Nau, W. M. Diffusion-Enhanced Förster Resonance Energy Transfer and the Effects of External Quenchers and the Donor Quantum Yield. *J. Phys. Chem. B* **2013**, *117*, 185−198.

(31) Karolczak, J.; Kowalska, D.; Lukaszewicz, A.; Maciejewski, A.; Steer, R. P. Photophysical Studies of Porphyrins and Metalloporphyrins: Accurate Measurements of Fluorescence Spectra and Fluorescence Quantum Yields for Soret Band Excitation of Zinc Tetraphenylporphyrin. *J. Phys. Chem. A* **2004**, *108*, 4570−4575.